

Waymo-3DSkelMo: A Multi-Agent 3D Skeletal Motion Dataset for Pedestrian Interaction Modeling in Autonomous Driving

Guangxun Zhu
g.zhu.1@research.gla.ac.uk
University of Glasgow
Glasgow, United Kingdom

Hang Dai
daihang@whu.edu.cn
Wuhan University
Wuhan, China
University of Glasgow
Glasgow, United Kingdom

Shiyu Fan
s.fan.1@research.gla.ac.uk
University of Glasgow
Glasgow, United Kingdom

Edmond S. L. Ho*
Shu-Lim.Ho@glasgow.ac.uk
University of Glasgow
Glasgow, United Kingdom

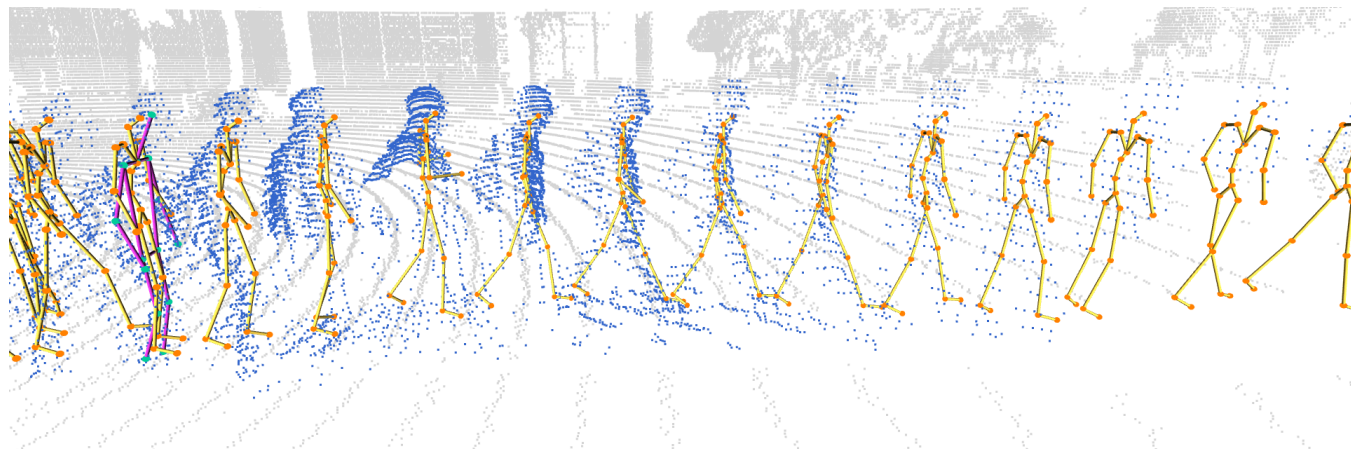


Figure 1: Waymo-3DSkelMo: A high-quality 3D Multi-pedestrian motion dataset created using human motion and shape priors from LiDAR range images in the Waymo perception dataset. (Blue) The point clouds, sampled every 0.5 seconds, of a pedestrian from the LiDAR range images. A 3D body mesh can be estimated from the partial LiDAR point cloud using a 3D human shape prior for each sample. (Purple) The Waymo dataset comes with very sparsely annotated 3D skeletal poses. (Yellow) Based on the skeletal poses extracted from the estimated body meshes, a motion prior is used to enhance the motion quality.

Abstract

Large-scale high-quality 3D motion datasets with multi-person interactions are crucial for data-driven models in autonomous driving to achieve fine-grained pedestrian interaction understanding in dynamic urban environments. However, existing datasets mostly rely on estimating 3D poses from monocular RGB video frames, which suffer from occlusion and lack of temporal continuity, thus resulting in unrealistic and low-quality human motion. In this paper, we introduce Waymo-3DSkelMo, the first large-scale dataset providing

high-quality, temporally coherent 3D skeletal motions with explicit interaction semantics, derived from the Waymo Perception dataset. Our key insight is to utilize 3D human body shape and motion priors to enhance the quality of the 3D pose sequences extracted from the raw LiDAR point clouds. The dataset covers over 14,000 seconds across more than 800 real driving scenarios, including rich interactions among an average of 27 agents per scene (with up to 250 agents in the largest scene). Furthermore, we establish 3D pose forecasting benchmarks under varying pedestrian densities, and the results demonstrate its value as a foundational resource for future research on fine-grained human behavior understanding in complex urban environments. The dataset and code will be available at <https://github.com/GuangxunZhu/Waymo-3DSkelMo>

*Corresponding author



This work is licensed under a Creative Commons Attribution-NonCommercial-ShareAlike 4.0 International License.

MM '25, Dublin, Ireland

© 2025 Copyright held by the owner/author(s).

ACM ISBN 979-8-4007-2035-2/2025/10

<https://doi.org/10.1145/3746027.3758273>

CCS Concepts

• **Computing methodologies** → *Machine learning*; **Computer vision**.

Keywords

Multi-person interaction, Pedestrian interaction, 3D Skeletal Motion, LiDRA, Motion dataset

ACM Reference Format:

Guangxun Zhu, Shiyu Fan, Hang Dai, and Edmond S. L. Ho. 2025. Waymo-3DSkelMo: A Multi-Agent 3D Skeletal Motion Dataset for Pedestrian Interaction Modeling in Autonomous Driving. In *Proceedings of the 33rd ACM International Conference on Multimedia (MM '25)*, October 27–31, 2025, Dublin, Ireland. ACM, New York, NY, USA, 7 pages. <https://doi.org/10.1145/3746027.3758273>

1 Introduction

Understanding interactions between intelligent agents (e.g. pedestrians and vehicles) and their surrounding environment is crucial for autonomous vehicles to achieve accurate perception and safe planning in dynamic urban ecosystems. Recent advances have demonstrated that interaction-aware perception systems produce significant breakthroughs in tasks such as pedestrian trajectory prediction [22] and 3D pose forecasting [16, 23].

The main challenge in interaction modeling lies in capturing the fine-grained dynamics of pedestrian behavior. Pedestrians, as indispensable participants in road environments, need special attention in the development of autonomous driving technologies. For example, they actively avoid collisions with other road users (e.g., pedestrians, vehicles, cyclists, etc.), while their movements are constrained by roads, traffic signs, and surrounding infrastructure. Inaccurate or coarse modeling can lead to incorrect predictions of the future trajectory of pedestrians, which may mislead autonomous vehicles to take actions in response to the situation.

Most existing works [1, 4, 17] model interactions between pedestrians using 2D locations, 2D poses, etc. Recently, some studies have attempted to incorporate 3D human poses to better capture motion dynamics [10, 18]. Compared to 2D data, 3D human pose provides richer spatial structure and depth information, offering a stronger foundation for fine-grained interaction modeling. However, due to the lack of fully annotated 3D data in existing public datasets on pedestrian interactions (see Table 1), researchers have been collecting multi-pedestrian 3D skeletal motion data by applying state-of-the-art 3D pose estimation from RGB image frames [10, 11], such as JRDB-GlobMultiPose (JRDB-GMP) [11] and MuPoTS-3D [15]. However, that resulted in poor motion quality due to the absence of temporal information from frame-based pose estimation and heavy occlusion when handling scenes with multiple pedestrians interacting with each other. Wang et al. [21] explored combining single-person and two-person motions as synthetic 3-person interaction using data from the high-quality CMU-MOCAP dataset [2] which was collected using optical Motion Capture (MOCAP) system. However, this results in a synthetic dataset with low diversity. There is also a stream of research that focuses on estimating 3D poses directly from noisy, sparse, and incomplete LiDAR point clouds. This process can introduce a lot of noise and lacks prior knowledge about the human body and motion [25]. Although some methods consider motion consistency via neighborhood enhancement for short-term coherence [26], their modeling remains spatially local without considering long-term or global temporal information.

To mitigate the challenges of data scarcity and enhance data quality, we present Waymo-3DSkelMo (Figure 1). To our best knowledge, this is the first large-scale dataset to provide high-quality 3D skeletal motions with explicit interaction semantics, all derived from raw LiDAR range images in the Waymo Open Dataset Perception Benchmark (hereafter referred to as Waymo) [19] which were captured from real-world outdoor scenarios. Our dataset overcomes the aforementioned issues by using human body shape priors through SMPL [13] mesh recovery and enhancing the naturalness of the 3D motion using human motion priors through Neural Motion Field (NeMF) [8]. Waymo-3DSkelMo thus bridges the gap between raw sensor data and interaction decoding requirements. Specifically, our dataset covers more than 14,000 seconds of recordings from over 800 real driving scenarios, capturing interactions among an average of 27 agents per scene and reaching 250 agents in the most crowded scenarios, providing abundant multi-agent interaction patterns for robust modeling. Moreover, our dataset is spatially and temporally synchronized with the original Waymo dataset, allowing seamless cross-modal integration with existing LiDAR/camera sensor data and annotations. Finally, to demonstrate the potential application of our dataset, we establish rigorous benchmarks for 3D pose forecasting, with protocols for short-term (1s) prediction across scenes with varying numbers of pedestrians.

Our contributions can be summarized as follows:

- We propose a new pipeline to adopt SMPL-based mesh recovery to acquire higher-quality 3D pose from raw LiDAR data and further enhance the motion quality using a motion prior trained with millions of frames.
- We release the first large-scale autonomous driving dataset featuring continuous, occlusion-robust 3D skeletal motions with explicit interaction semantics, fully aligned with the Waymo dataset.
- We benchmark 3D pose forecasting performance across scenes with varying pedestrian densities to facilitate in-depth analysis of interaction-aware motion prediction and serve as a foundation for future research on fine-grained human behavior understanding in complex driving environments.

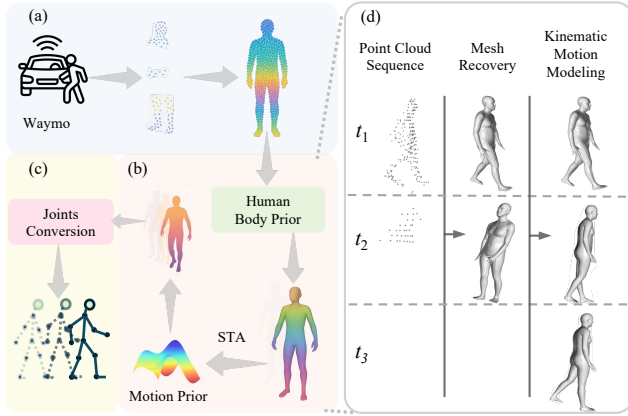
2 Description of the dataset

Our dataset contains over 14,000 seconds of pedestrian 3D skeletal motion sequences across 837 distinct real-world scenes, with an average of 27 agents interacting per scene. The number of pedestrians per scene ranges from 1 to over 250. The raw data are sourced from the training and validation sets of the Waymo dataset. Please refer to Section 3.1 for the details of the original Waymo dataset.

Table 1 presents a quantitative comparison between the combined training and validation splits of the original Waymo dataset and our proposed Waymo-3DSkelMo. Note that test sets are excluded due to licensing restrictions. Both datasets share the same 837 scenes containing pedestrians. While Waymo-3DSkelMo shows a slightly lower total duration (14,419 s vs. 14,421 s) and number of pedestrians per scene (27.1 vs. 27.6 average; 250 vs. 253 maximum) compared to the original Waymo dataset, this is primarily due to missing point cloud data in the original dataset that covers the full duration of some pedestrian motion sequences. In such

Table 1: Comparison of statistics between the newly proposed Waymo-3DSkelMo and existing human pose forecasting datasets

	Waymo-3DSkelMo (Ours)	Waymo [19]	MuPoTS-3D [15]	CMU-Mocap (UMPM) [16]	JRDB-GMP [11]
Scenes w/pedestrains	837	837	20	Partially synthetic	27
Duration (s)	14419	14421	267	4,000	1863
avg. pedestrians #	27.1	27.6	3	3	6.8
max. pedestrians #	250	253	3	3	24
avg. displacement (m)	10.41	10.33	0.55	0.63	0.76
3D poses # (@10 fps)	2,438,145	9,976	8,010	120,000	400,000
Collection method	LiDAR PE + motion enhancement	Manual annotation	RGB Image PE	Optical MOCAP sequences + mixing	RGB Image PE
(PE=Pose Estimation)					

**Figure 2: Overview of our pipeline. (a) Point clouds are first extracted from the range images of all five Waymo LiDAR sensors, then transformed into a world coordinate system and fused into a unified point cloud representation. (b) Mesh recovery is performed on all point clouds using a human-body prior, followed by motion generation via a motion prior. (c) Regressing SMPL parameters to skeletal motions. (d) An example of different quality of point cloud and 3D pose.**

cases, generating reliable and temporally consistent 3D annotations is infeasible, and those sequences are therefore excluded from our version, leading to a higher average displacement (10.41 *m* vs. 10.33 *m*). In particular, the original Waymo dataset provides only about 10,000 manually annotated 3D poses for pedestrians across all scenes, resulting in sparse and isolated ground-truth labels. On the other hand, Waymo-3DSkelMo offers dense 3D skeletal motion annotations for all pedestrians at every time step, totaling 2,438,145 frame-level annotations (@10 fps) generated using human body and motion priors. This dense supervision enables fine-grained temporal modeling and mitigates the sparsity and inconsistency present in the original keypoint annotations.

Moreover, both datasets contain highly interactive scenes with up to 250 pedestrians appearing in a single scene, which makes Waymo-3DSkelMo particularly valuable for modeling large-scale multi-agent interaction dynamics in autonomous driving contexts.

Compared to MuPoTS-3D [15], CMU-Mocap (UMPM) [16], and JRDB-GMP [11], which are also densely annotated, Waymo-3DSkelMo offers significantly larger scale, richer interactions, and more dynamic motion. While the three datasets contain on average only 3 to 6.8 pedestrians per scene with a duration of up to 4,000 seconds, Waymo-3DSkelMo spans over 14,000 seconds, includes up to 250 pedestrians per scene (27.1 on average), and achieves a higher average displacement of 10.41 meters, reflecting longer trajectories which contain more interactions among the pedestrians.

In addition, our dataset provides detailed 3D pedestrian motion annotations in two main formats: keypoint-based data and SMPL mesh data. The keypoint format includes 3D coordinates of human skeletal joints, while the SMPL format offers a comprehensive parametric human mesh capturing detailed body shape and pose. To accommodate different research needs, we supply the dataset at two frame rates: 30 fps and 10 fps. The 10 fps version is temporally synchronized with the original Waymo dataset, with aligned timestamps, making it suitable for use as ground truth annotations.

3 Dataset Generation Process

An overview of our 3D skeletal motion dataset generation is illustrated in Figure 2. Our dataset described in Section 2 is generated from the raw LiDAR range images provided in the Waymo dataset [19]. First, point clouds are extracted from the range images captured from all five Waymo LiDAR sensors, reprojected into a common world-coordinate frame via extrinsic calibration, and merged into a unified 3D point cloud representation. We then utilise LiDAR-HMR [6] to recover 3D Human Mesh based on a 3D human shape prior from the raw LiDAR data. The output of LiDAR-HMR contains noisy and missing data, and we mitigate these issues by spatiotemporal alignment. We further take advantage of using 3D human skeletal motion prior to improve the motion quality of the refined output using the Neural Motion Field (NeMF) [8]. The details are explained in the following subsections.

3.1 Waymo Perception Dataset

The Waymo Open Dataset Perception Benchmark [19] introduced human keypoint annotations in version 1.3.2, which includes LiDAR range images along with corresponding camera images. For our experiments, we use version 2.0 for training and validation. This version provides annotations of 14 keypoints (as a pose, from nose to ankle) per pedestrian. The training set contains 8,125 annotated

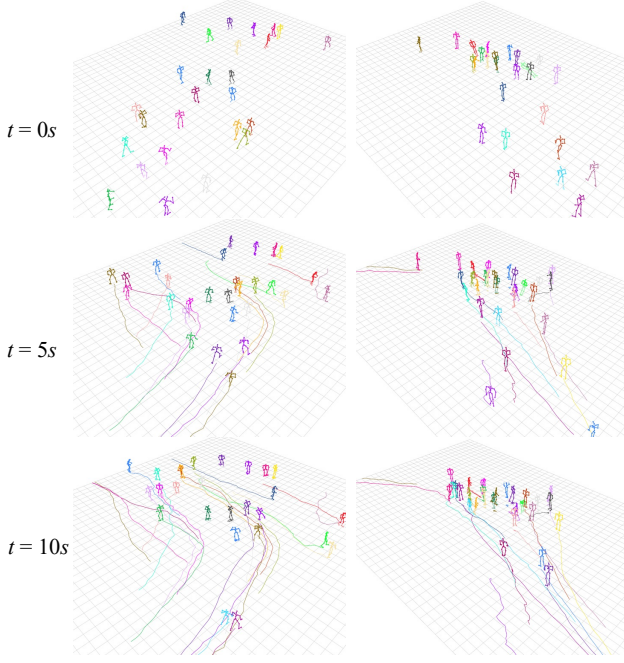


Figure 3: Example scenes from the Waymo-3DSkelMo dataset, illustrating its multi-agent interaction nature.

poses, while the validation set includes 1,873. However, the raw LiDAR point clouds often suffer from sparsity and noise, especially at longer ranges, resulting in missing or unevenly distributed 3D points around occluded limbs and small body parts. These quality issues make it difficult to obtain reliable 3D poses from the raw LiDAR data.

3.2 3D Human Mesh Recovery

To accurately capture human body shape and pose from sparse, noisy, and incomplete LiDAR data, we adopt LiDAR-HMR [6], a state-of-the-art method for 3D human mesh recovery. LiDAR-HMR leverages a parametric human body model (SMPL) as a prior to reconstruct detailed 3D meshes from raw LiDAR range images, allowing robust recovery even under occlusions and partial observations.

As shown in Figure 2 (d), in our pipeline, LiDAR-HMR processes LiDAR observations of each pedestrian frame-by-frame, treating each pedestrian at every timestamp as an individual instance. We perform human mesh recovery on all point clouds, even if a point cloud contains only a single point. For high-quality and relatively complete point clouds (e.g., at t_1 in Figure 2), LiDAR-HMR can generate accurate and reliable meshes. However, when point clouds are incomplete or noisy, the recovered meshes often suffer from issues such as inconsistent orientations, incorrect heights, and poses that are not consistent with the point cloud data or temporal motion patterns (e.g., at t_2 in Figure 2). Moreover, in the absence of point cloud data, mesh recovery is not feasible (e.g., at t_3 in Figure 2).

3.3 Spatiotemporal Alignment

To achieve more coherent motion, we perform spatiotemporal alignment (STA) through temporal interpolation and Frenet frame [5] transformation. Specifically, we first apply spherical linear interpolation (slerp) for joint rotations and linear interpolation for translations to fill missing frames in pedestrian sequences. The data is then upsampled to 30 fps to match the next processing step. To resolve inconsistent global orientations, we adopt the Frenet frame, which constructs a local coordinate system along motion trajectories using tangent (T), normal (N), and binormal (B) vectors, ensuring stable orientation representation relative to movement direction. Together, these spatiotemporal alignment steps yield smoother, consistently oriented 3D motion that is better suited for subsequent processing. The improvements are highlighted in Table 2.

3.4 Neural Motion Fields

To further overcome temporal inconsistencies and missing frames in the recovered 3D meshes, we utilize Neural Motion Fields (NeMF) [8]. NeMF offers a continuous and smooth representation of kinematic motion, enabling the interpolation of missing data and enforcing realistic motion dynamics. Since NeMF is pre-trained using the AMASS [14] dataset which contains over 40 hours of high-quality 3D motion data (>11,000 motion sequences) collected from over 300 subjects, this enables us to use NeMF as a generic motion prior to enhance the quality of the motion sequences.

Given the interpolated poses, we first encode the 3D skeletal pose sequence into NeMF motion latent representation (z_l for the *local* pose relative to the root joint and z_g for *global* translation of the root joint) using the pre-trained NeMF encoder and optimize it based on the energy function:

$$z_l^*, z_g^* = \underset{z_l, z_g}{\operatorname{argmin}} \sum_{\mathcal{T}} \lambda_{rot} \mathcal{L}_{rot} + \lambda_{ori} \mathcal{L}_{ori} + \lambda_{pos} \mathcal{L}_{pos} + \lambda_{trans} \mathcal{L}_{trans} \quad (1)$$

where \mathcal{L}_{rot} and \mathcal{L}_{pos} are the L_1 losses on the 6D rotations [27] and the 3D local positions of all joints, \mathcal{L}_{ori} and \mathcal{L}_{trans} are the L_1 losses on the orientation and translation of the root joint, respectively, and \mathcal{T} is a set of all interpolated frames from the spatiotemporal alignment (Section 3.3). The L_1 losses are calculated between the interpolated 3D skeletal motion sequence and the motion decoded from the intermediate NeMF representation (i.e. z_l^* and z_g^*). Furthermore, the loss terms for keyframes (those with ground-truth annotations in the original Waymo dataset) are weighted 10× higher than those for other frames, in order to mitigate error accumulation and obtain motion sequences that better reflect realistic human movements. By this, the resultant motion will be as similar to the interpolated motion as possible while preserving the naturalness as represented in the NeMF. We empirically found $\lambda_{rot} = \lambda_{ori} = 1$ and $\lambda_{pos} = \lambda_{trans} = 10$ yield the best outcomes.

3.5 Generation results and evaluation

To validate the effectiveness of our pipeline, we conduct comprehensive comparisons across four paradigms:

- **LiDAR-HMR Raw:** Direct outputs from the LiDAR-HMR without refinement.

- **Linear Interpolation:** Frame-wise linear filling of missing poses within LiDR-HMR output.
- **CondMDI-based:** Motion inbetweening via the state-of-the-art CondMDI model [3], using LiDAR-HMR outputs as keyframes to complete the missing frames.
- **Ours:** Full pipeline with NeMF-based motion reconstruction.

To quantitatively evaluate motion quality, we compare the motion generated using the aforementioned methods by four established metrics: Fréchet Inception Distance (FID) [3, 8, 24], which measures the distance between the distribution of generated motions and that of real motions from the HumanML3D dataset [7] to indicate overall realism; Jittering [12, 24], computed as the average L_2 norm of joint acceleration vectors across all joints and frames, to quantify frame-to-frame smoothness; Mean Per Joint Position Error (MPJPE) [6, 25], defined as the mean Euclidean distance between the generated joint position and the ground-truth position at frames with annotated corresponding 3D keypoints in Waymo; and Foot Skating Ratio (FS) [3, 8, 24], the percentage of frames in which foot-ground penetration exceeds 2 cm, to assess the physical plausibility of the motion.

Quantitative results are presented in Table 2. Our method achieves the lowest FID in both settings (12.2387 w/o Frenet, 10.4501 w/ Frenet), indicating that its motion distribution resembles the real pedestrian data the most closely. The improvement in FID achieved through Frenet alignment indicates that resolving inconsistent global orientations leads to motion sequences that more accurately reflect realistic human movement patterns. It also attains the lowest foot-skating ratios (0.030393 w/o Frenet, 0.034975 w/ Frenet), reflecting superior contact realism, though the slight degradation under Frenet alignment results from correcting systematic orientation drift. The lowest joint-acceleration jitter (0.047769 w/o Frenet, 0.047220 w/ Frenet) further demonstrates smoother trajectories, particularly after applying Frenet-frame corrections.

Although raw LiDAR-HMR and linear interpolation preserve joint positions most accurately (0.0869 w/o Frenet, 0.1263 w/ Frenet), they suffer from poor pose expressiveness and temporal stability. In contrast, slightly increase in pose position error in our pipeline (0.1391 w/o Frenet, 0.1705 w/ Frenet) is outweighed by substantial gains in temporal coherence, and anatomical plausibility—benefits that are further enhanced by orientation correction. CondMDI, on the other hand, underperforms across all metrics, as its reliance on keyframe quality and distribution propagates noise and leads to inconsistent motion between frames.

Additionally, Figure 3 visualizes some scenes from the Waymo-3DSkelMo dataset. Even in high-density scenarios (up to 30 pedestrians), the motion remains remarkably smooth and collision-free. The dataset spans pedestrian motions of both long and short distances and showcases extensive agent-to-agent interaction in terms of both trajectories and local poses.

4 Benchmarking on the dataset

To validate the effectiveness of our dataset, we benchmark it using TBIFormer [16], an interaction-aware 3D pose forecasting model.

4.1 Dataset

We follow the original training and validation splits of Waymo, specifically selecting scenes containing 2 to 5 pedestrians for benchmarking, as these represent typical urban interaction scenarios. To align with TBIFormer’s temporal resolution, the NeMF-based generated sequences, which are originally at 30 fps, are downsampled to 25 fps. For short-term prediction, we use 2 seconds (50 frames) of historical observation to predict 1 second (25 frames) of future poses. Overlapping segments with consistent pedestrian counts are then identified through timestamp alignment. Subsequently, a sliding window with a duration of 3 seconds (75 frames) and a step size of 50 frames is applied to extract clips. In addition, data augmentation techniques are employed, including global rotations around the vertical axis in discrete steps of 10° , Gaussian noise ($\sigma = 0.01$ m) added to joint positions, and random spatial scaling between 0.9 and 1.1, to enhance the diversity of the dataset.

4.2 Implementation details

We implement our framework in PyTorch, and the experiments are performed on a single Nvidia GeForce RTX 4090 GPU. We train our model for 50 epochs using the ADAM optimizer with a batch size of 32, a learning rate of 0.00002, and a dropout rate of 0.2. All other settings remain consistent with TBIFormer. Notably, separate models are trained for different numbers of pedestrians to better accommodate the variations in interaction distributions.

4.3 Evaluation Metrics

We adopt the same evaluation metrics as TBIFormer[16]: the Joint Position Error (JPE), Aligned Mean Per Joint Position Error (APE) and Final Displacement Error (FDE). JPE measures the average per-joint Euclidean distance between predicted and ground-truth poses across all pedestrians, while APE further removes global translation by aligning root joints before computing JPE. FDE assesses the accuracy of predicted root positions at the final time step.

4.4 Results

Table 3 presents the short-horizon prediction errors of TBIFormer under different numbers of persons, evaluated by JPE, APE, and FDE at 0.2s, 0.6s, 1.0s time horizons, as well as overall average errors.

As expected, all three metrics increase with prediction horizon, reflecting growing uncertainty in longer-term forecasting. Notably, settings with three and four pedestrians yield the lowest overall JPE (172 mm and 191 mm, respectively) and FDE (110 mm and 140 mm, respectively), indicating that modeling moderate levels of interactions between pedestrians enhances predictive accuracy. In contrast, both overly sparse and overly dense pedestrian configurations present challenges. However, the APE is lowest (109 mm) in the two-person case, which indicates that adding more pedestrian interactions can actually introduce extra noise into individual joint predictions, raising the absolute error when three to five people are involved.

In [16], the pose forecasting performance on the CMU-Mocap [2] (merged with UPM [20]) (3 persons) and MuPoTS-3D [15] (2 to 3 persons) datasets was reported. On CMU-Mocap (UPM),

Table 2: Quantitative comparison of motion generation methods with and without Frenet-frame alignment. Metrics marked with ↓ indicate that lower values are better. Within each setting (with/without Frenet), the best result for each metric is highlighted in bold.

Setting	Method	FID ↓	Foot Skating ↓	MPJPE (m) ↓	Jittering (m/f ²) ↓
w/o Frenet	LiDAR-HMR Raw	15.5387	0.032430	0.0869	0.315535
	Linear Interpolation	19.1160	0.032525	0.0869	0.250194
	CondMDI-based	14.6586	0.051199	0.8241	0.250889
	NeMF-based (Ours)	12.2387	0.030393	0.1391	0.047769
Frenet	LiDAR-HMR Raw	15.8628	0.033833	0.1263	0.314766
	Linear Interpolation	19.9499	0.033603	0.1263	0.249554
	CondMDI-based	16.7842	0.038380	0.8870	0.228974
	NeMF-based (Ours)	10.4501	0.034975	0.1705	0.047220

Table 3: Results of JPE, APE and FDE (in mm) under different number of persons settings. We compare short-term predictions using TBIFormer across varying person interactions.

	2 persons				3 persons				4 persons				5 persons			
	0.2s	0.6s	1.0s	Overall	0.2s	0.6s	1.0s	Overall	0.2s	0.6s	1.0s	Overall	0.2s	0.6s	1.0s	Overall
JPE	110	366	504	326	89	190	237	172	98	200	276	191	113	261	368	247
APE	72	130	124	109	78	141	157	125	83	137	152	124	90	149	153	131
FDE	80	313	469	287	51	120	159	110	56	143	221	140	67	199	316	194

TBIFormer achieved an overall JPE = 107, APE = 76 and FDE = 74, while achieving an overall JPE = 195, APE = 121 and FDE = 63 on MuPoTS-3D. Note that the CMU-Mocap (UMPM) dataset contains a large amount of synthetic 3-person data by mixing single-person and two-person walking motions together as in [21], which results in a low diversity dataset. It can be seen that TBIFormer performed particularly well on this less-challenging dataset. The performance of TBIFormer on MuPoTS-3D and our dataset is similar in overall JPE and APE, while there is a bigger performance gap in FDE. The results show that TBIFormer’s performance on our dataset is comparable to other datasets, and our work will provide the community with a more challenging dataset for future research.

It is important to note that our tests only consider interactions between pedestrians and leave out cars, bicycles, and other static or moving objects in the scene. Those missing factors can affect the walking paths of pedestrians which introduce variation and degrade predictive performance under certain conditions.

5 Conclusion

In this work, we present Waymo-3DSkelMo, the first large-scale dataset enabling fine-grained interaction modeling through high-quality 3D skeletal motions in real-world driving scenarios. By integrating human shape priors and neural motion field, our dataset provides occlusion-robust and temporally coherent 3D skeletal motions with explicit interaction semantics while maintaining full spatiotemporal alignment with Waymo dataset. Comprising 14,000 seconds of recordings across 800+ diverse scenarios (1-250+ agents/scene), it establishes a foundational resource validated through 3D pose forecasting benchmarks for modeling complex multi-pedestrian behaviors. Future enhancements will incorporate advanced models

for point cloud alignment [9] for pose estimation as well as evaluating the impact on the performance of using different 3D body shape and motion priors.

6 Licensing and Access

The enhanced 3D skeletal motion sequences are publicly available for non-commercial use, which also aligns with the Waymo Open Dataset [19]. Similarly, we will align with the Waymo dataset on limiting the model architectures for non-commercial distribution only, which means the user may publish, in whole or in part, trained model architectures, including weights and biases, developed using our dataset for non-commercial purposes.

We will also open-source the Python implementation for the motion enhancement. All material, including code and dataset, will be made available under Creative Commons BY-NC-SA 4.0 license.

7 Reproducibility and Supplementary Materials

As stated in Section 6, the code for motion enhancement will be made available as an open-source project. Instructions will be given for accessing the other models and resources used in this project to reproduce the experimental results and the dataset.

8 Ethical Considerations and Privacy

The input data source of our proposed pipeline is fully anonymized. Therefore, there are no ethical considerations or privacy issues.

Acknowledgments

Guangxun Zhu is supported by the funding from the China Scholarship Council (CSC).

References

- [1] Mohsen Azarmi, Mahdi Rezaei, and He Wang. 2025. PIP-Net: Pedestrian Intention Prediction in the Wild. *IEEE Transactions on Intelligent Transportation Systems* 26, 7 (2025), 9824–9837. doi:10.1109/TITS.2025.3570794
- [2] CMU. 2003. CMU Graphics Lab Motion Capture Database. <http://mocap.cs.cmu.edu/>
- [3] Setareh Cohan, Guy Tevet, Daniele Reda, Xue Bin Peng, and Michiel van de Panne. 2024. Flexible Motion In-betweening with Diffusion Models. In *ACM SIGGRAPH 2024 Conference Papers* (Denver, CO, USA) (SIGGRAPH '24). Association for Computing Machinery, New York, NY, USA, Article 69, 9 pages. doi:10.1145/3641519.3657414
- [4] Luca Crosato, Hubert P. H. Shum, Edmond S. L. Ho, and Chongfeng Wei. 2023. Interaction-Aware Decision-Making for Automated Vehicles Using Social Value Orientation. *IEEE Transactions on Intelligent Vehicles* 8, 2 (2023), 1339–1349. doi:10.1109/ITV.2022.3189836
- [5] Manfredo P Do Carmo. 2016. *Differential geometry of curves and surfaces: revised and updated second edition*. Courier Dover Publications.
- [6] Bohao Fan, Wenzhao Zheng, Jianjiang Feng, and Jie Zhou. 2023. LiDAR-HMR: 3D Human Mesh Recovery from LiDAR. *arXiv preprint arXiv:2311.11971* (2023).
- [7] Chuan Guo, Shihao Zou, Xinxin Zuo, Sen Wang, Wei Ji, Xingyu Li, and Li Cheng. 2022. Generating diverse and natural 3d human motions from text. In *Proceedings of the IEEE/CVF conference on computer vision and pattern recognition*. 5152–5161.
- [8] Chengan He, Jun Saito, James Zachary, Holly Rushmeier, and Yi Zhou. 2022. NeMF: Neural Motion Fields for Kinematic Animation. In *Advances in Neural Information Processing Systems*, S. Koyejo, S. Mohamed, A. Agarwal, D. Belgrave, K. Cho, and A. Oh (Eds.), Vol. 35. Curran Associates, Inc., 4244–4256. https://proceedings.neurips.cc/paper_files/paper/2022/file/1b3750390ca8b931fb9ca988647940cb-Paper-Conference.pdf
- [9] Pengpeng Hu, Edmond S. L. Ho, and Adrian Munteanu. 2023. AlignBodyNet: Deep Learning-Based Alignment of Non-Overlapping Partial Body Point Clouds From a Single Depth Camera. *IEEE Transactions on Instrumentation and Measurement* 72 (2023), 1–9. doi:10.1109/TIM.2022.3222501
- [10] Jaewoo Jeong, Seohye Lee, Daehee Park, Giwon Lee, and Kuk-Jin Yoon. 2025. Multi-modal Knowledge Distillation-based Human Trajectory Forecasting. In *2025 IEEE/CVF Conference on Computer Vision and Pattern Recognition (CVPR)*.
- [11] Jaewoo Jeong, Daehee Park, and Kuk-Jin Yoon. 2024. Multi-Agent Long-Term 3D Human Pose Forecasting via Interaction-Aware Trajectory Conditioning. In *2024 IEEE/CVF Conference on Computer Vision and Pattern Recognition (CVPR)*. 16975–16984. doi:10.1109/CVPR52733.2024.00160
- [12] Korrawe Karunratanakul, Konpat Preechakul, Supasorn Suwajanakorn, and Siyu Tang. 2023. Guided motion diffusion for controllable human motion synthesis. In *Proceedings of the IEEE/CVF International Conference on Computer Vision*. 2151–2162.
- [13] Matthew Loper, Naureen Mahmood, Javier Romero, Gerard Pons-Moll, and Michael J Black. 2023. SMPL: A skinned multi-person linear model. In *Seminal Graphics Papers: Pushing the Boundaries, Volume 2*. 851–866.
- [14] Naureen Mahmood, Nima Ghorbani, Nikolaus F. Troje, Gerard Pons-Moll, and Michael Black. 2019. AMASS: Archive of Motion Capture As Surface Shapes. In *2019 IEEE/CVF International Conference on Computer Vision (ICCV)*. 5441–5450. doi:10.1109/ICCV.2019.00554
- [15] Dushyant Mehta, Oleksandr Sotnychenko, Franziska Mueller, Weipeng Xu, Srinath Sridhar, Gerard Pons-Moll, and Christian Theobalt. 2018. Single-Shot Multi-person 3D Pose Estimation from Monocular RGB. In *2018 International Conference on 3D Vision (3DV)*. IEEE Computer Society, Los Alamitos, CA, USA, 120–130. doi:10.1109/3DV.2018.00024
- [16] Xiaogang Peng, Siyuan Mao, and Zizhao Wu. 2023. Trajectory-aware body interaction transformer for multi-person pose forecasting. In *Proceedings of the IEEE/CVF conference on computer vision and pattern recognition*. 17121–17130.
- [17] Amir Rasouli and Iuliia Kotseruba. 2023. PedFormer: Pedestrian Behavior Prediction via Cross-Modal Attention Modulation and Gated Multitask Learning. In *2023 IEEE International Conference on Robotics and Automation (ICRA)*. 9844–9851. doi:10.1109/ICRA48891.2023.10161318
- [18] Saeed Saadatnejad, Yang Gao, Kaouthar Messaoud, and Alexandre Alahi. 2024. Social-Transmotion: Promptable Human Trajectory Prediction. In *International Conference on Learning Representations (ICLR)*.
- [19] Pei Sun, Henrik Kretschmar, Xerxes Dotiwalla, Aurelien Chouard, Vijaysai Patnaik, Paul Tsui, James Guo, Yin Zhou, Yuning Chai, Benjamin Caine, Vijay Vasudevan, Wei Han, Jiquan Ngiam, Hang Zhao, Aleksei Timofeev, Scott Ettinger, Maxim Krivokon, Amy Gao, Aditya Joshi, Yu Zhang, Jonathon Shlens, Zhifeng Chen, and Dragomir Anguelov. 2020. Scalability in Perception for Autonomous Driving: Waymo Open Dataset. In *Proceedings of the IEEE/CVF Conference on Computer Vision and Pattern Recognition (CVPR)*.
- [20] N.P. van der Aa, X. Luo, G.J. Giezeman, R.T. Tan, and R.C. Veltkamp. 2011. UMPM benchmark: A multi-person dataset with synchronized video and motion capture data for evaluation of articulated human motion and interaction. In *2011 IEEE International Conference on Computer Vision Workshops (ICCV Workshops)*. 1264–1269. doi:10.1109/ICCVW.2011.6130396
- [21] Jiashun Wang, Huazhe Xu, Medhini Narasimhan, and Xiaolong Wang. 2021. Multi-person 3D motion prediction with multi-range transformers. In *Proceedings of the 35th International Conference on Neural Information Processing Systems (NIPS '21)*. Curran Associates Inc., Red Hook, NY, USA, Article 462, 14 pages.
- [22] Conghao Wong, Beihao Xia, Ziqian Zou, Yulong Wang, and Xinge You. 2024. SocialCircle: Learning the Angle-based Social Interaction Representation for Pedestrian Trajectory Prediction. In *2024 IEEE/CVF Conference on Computer Vision and Pattern Recognition (CVPR)*. 19005–19015. doi:10.1109/CVPR52733.2024.01798
- [23] Peng Xiao, Yi Xie, Xuemiao Xu, Weihong Chen, and Huaidong Zhang. 2024. Multi-person Pose Forecasting with Individual Interaction Perceptron and Prior Learning. In *European Conference on Computer Vision*. Springer, 402–419.
- [24] Wenning Xu, Shiyu Fan, Paul Henderson, and Edmond S. L. Ho. 2025. Multi-Person Interaction Generation from Two-Person Motion Priors. In *Proceedings of the Special Interest Group on Computer Graphics and Interactive Techniques Conference Papers (SIGGRAPH Conference Papers '25)*. Association for Computing Machinery, New York, NY, USA, Article 113, 11 pages. doi:10.1145/3721238.3730688
- [25] Dongqiangzi Ye, Yufei Xie, Weijia Chen, Zixiang Zhou, Lingting Ge, and Hassan Foroosh. 2024. LPFormer: LiDAR pose estimation transformer with multi-task network. In *2024 IEEE International Conference on Robotics and Automation (ICRA)*. IEEE, 16432–16438.
- [26] Jingyi Zhang, Qihong Mao, Guosheng Hu, Siqi Shen, and Cheng Wang. 2024. Neighborhood-enhanced 3D human pose estimation with monocular LiDAR in long-range outdoor scenes. In *Proceedings of the AAAI Conference on Artificial Intelligence*, Vol. 38. 7169–7177.
- [27] Yi Zhou, Connelly Barnes, Jingwan Lu, Jimei Yang, and Hao Li. 2019. On the Continuity of Rotation Representations in Neural Networks. In *2019 IEEE/CVF Conference on Computer Vision and Pattern Recognition (CVPR)*. 5738–5746. doi:10.1109/CVPR.2019.00589